Electron scattering and doping mechanisms in solid-phase-crystallized In2O3:H prepared by atomic layer deposition

ACS APPLIED MATERIALS & INTERFACES

Research Article

www.acsami.org

Electron Scattering and Doping Mechanisms in Solid-Phase-Crystallized In_2O_3:H Prepared by Atomic Layer Deposition

Bart Macco,*[,†] Harm C. M. Knoops,[†] and Wilhelmus M. M. Kessels[†,‡]

[†]Department of Applied Physics, Eindhoven University of Technology, P.O. Box 513, 5600 MB Eindhoven, The Netherlands

[‡]Solliance Solar Research, High Tech Campus 5, 5656 AE Eindhoven, The Netherlands

Supporting Information

ABSTRACT: Hydrogen-doped indium oxide (In_2O_3:H) has recently emerged as an enabling transparent conductive oxide for solar cells, in particular for silicon heterojunction solar cells because its high electron mobility (>100 $cm^2/(V\,s)$) allows for a simultaneously high electrical conductivity and optical transparency. Here, we report on high-quality In_2O_3:H prepared by a low-temperature atomic layer deposition (ALD) process and present insights into the doping mechanism and the electron scattering processes that limit the carrier mobility in such films. The process consists of ALD of amorphous In_2O_3:H at 100 °C and subsequent solid-phase crystallization at 150−200 °C to obtain large-grained polycrystalline In_2O_3:H films. The changes in optoelectronic properties upon crystallization have been monitored both electrically by Hall measurements and optically by analysis of the Drude response. After crystallization, an excellent carrier mobility of 128 ± 4 $cm^2/(V\,s)$ can be obtained at a carrier density of 1.8 × 10^{20} cm^{-3}, irrespective of the annealing temperature. Temperature-dependent Hall measurements have revealed that electron scattering is dominated by unavoidable phonon and ionized impurity scattering from singly charged H-donors. Extrinsic defect scattering related to material quality such as grain boundary and neutral impurity scattering was found to be negligible in crystallized films indicating that the carrier mobility is maximized. Furthermore, by comparison of the absolute H-concentration and the carrier density in crystallized films, it is deduced that <4% of the incorporated H is an active dopant in crystallized films. Therefore, it can be concluded that inactive H atoms do not (significantly) contribute to defect scattering, which potentially explains why In_2O_3:H films are capable of achieving a much higher carrier mobility than conventional In_2O_3:Sn (ITO).

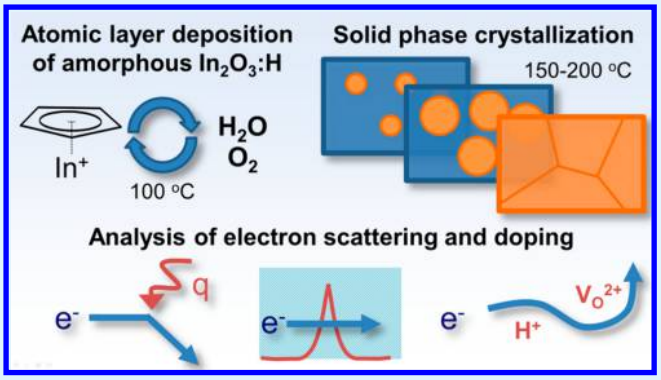

KEYWORDS: *Atomic layer deposition, transparent conductive oxide, spectroscopic ellipsometry, carrier mobility, solid-phase crystallization, doping, ionized impurity scattering, phonon scattering*

INTRODUCTION

Tin-doped indium oxide (In_2O_3:Sn or ITO) has become the most widely used transparent conductive oxide (TCO) in a wide range of optoelectronic applications including displays and solar cells. The key advantage of In_2O_3:Sn is its relatively high electron mobility μ. A high electron mobility allows for a high electrical conductivity at a lower carrier density, thereby mitigating free carrier absorption (FCA) in the infrared. In_2O_3:Sn films are usually prepared by sputtering, and typical values for the mobility encountered in literature lie in the 20−40 $cm^2/(V\,s)$ range.[1]

Recently, H doping of In_2O_3 has gained significant interest over traditional Sn doping. This development was sparked in 2007, when Koida et al. demonstrated that H-doped indium oxide (In_2O_3:H) films can exhibit an extremely high Hall mobility of 130 $cm^2/(V\,s)$ at moderate carrier densities of 1−2 × 10^{20} cm^{-3}.[2,3] Their process consisted of the deposition of amorphous In_2O_3:H at room temperature by rf magnetron sputtering using an In_2O_3 ceramic target, with the addition of H_2O vapor as a source of H doping. To obtain the excellent film properties, the films were subjected to a postdeposition anneal, which led to solid-phase crystallization (SPC) of the films. Although H doping results in a resistivity similar to that typical for Sn doping, the FCA is strongly reduced because of a lower carrier density and a higher mobility. This makes In_2O_3:H particularly promising for optoelectronic applications in which FCA is an issue, such as silicon heterojunction (SHJ) solar cells.[4] Indeed, as various authors have shown, the reduced FCA can significantly enhance the short-circuit current density J_{sc} of a SHJ solar cell.[5−8]

These experimental results were soon followed by further theoretical and experimental work to explore the doping mechanism and scattering processes limiting the mobility in In_2O_3:H. First, the donor nature of H in In_2O_3 was confirmed by ab initio calculations by Van de Walle and co-workers, who demonstrated that the hydrogen donor state (either interstitial

Received: May 21, 2015
Accepted: July 13, 2015
Published: July 13, 2015

DOI: 10.1021/acsami.5b04420
ACS Appl. Mater. Interfaces 2015, 7, 16723−16729

or substitutional) is energetically more favorable than an oxygen vacancy.[9] Second, Preissler et al. have performed a detailed experimental and theoretical investigation of the scattering processes in single-crystal In_2O_3 for a large range of carrier densities (7×10^{16}–1×10^{21} cm^{-3}).[10] Key findings were that optical phonon scattering is dominant for carrier densities $<10^{20}$ cm^{-3}, whereas ionized impurity scattering is dominant for higher carrier densities. At intermediate carrier densities of $1–2 \times 10^{20}$ cm^{-3}, their model predicts a local maximum in mobility (~90 $cm^2/(V\,s)$). This maximum is due to a balance in decreasing phonon scattering by increased screening of optical phonons and increased ionized impurity scattering with increasing carrier density. This predicted local maximum in mobility at carrier densities of $1–2 \times 10^{20}$ cm^{-3} was also found experimentally, but the experimental values exceeded their predicted local maximum in mobility of ~90 $cm^2/(V\,s)$. This was tentatively attributed to an underestimated screening of the optical phonons.[10]

In 2011, Libera et al. demonstrated a low-temperature (≥100 °C) atomic layer deposition (ALD) process for In_2O_3 using cyclopentadienyl indium (InCp) and a combination of both H_2O and O_2 as reactants.[11] Depending on the growth temperature and reactant exposure sequence, either amorphous or polycrystalline films were obtained. The highest mobility (111 $cm^2/(V\,s)$) was obtained using a simultaneous exposure of the film to O_2 and H_2O during the reactant step at a deposition temperature of 140 °C, which is just above the transition temperature from amorphous to polycrystalline growth. However, hydrogen incorporation, postannealing, or doping mechanisms were not investigated for this process at that time.

Recently, we demonstrated that In_2O_3:H films of superior quality can be made by an approach combining the work of Koida et al. and Libera et al.[12] Amorphous In_2O_3:H films of 75 nm were deposited by ALD using InCp and a combination of both H_2O and O_2 at a substrate temperature of 100 °C. H was unintentionally incorporated during the ALD process, leading to a H concentration of 4.2 atomic percent (at. %). By subsequent thermal crystallization at 200 °C, crystal grains that extend over the full film thickness and are a few hundred nanometers in lateral size were obtained. This, together with a high in-grain crystal quality, resulted in films with a very high Hall mobility (138 $cm^2/(V\,s)$), a moderate carrier density (1.8×10^{20} cm^{-3}), and a low resistivity (0.27 mΩ cm).[12] Furthermore, besides excellent material quality, one of the main merits of the preparation process using ALD and SPC is the absence of plasma-induced damage to the underlying layers that is typically found in conventional sputter deposition.[13−15] Moreover, this carrier density is in the range of the predicted local maximum by Preissler et al., yet the mobility exceeds their predicted value. This renders these films ideally suited for further study of the electron scattering mechanisms limiting the carrier mobility of In_2O_3:H.

This work aims to extend the understanding of the factors that govern the carrier density and limit the carrier mobility in ALD In_2O_3:H films by analysis of the doping and the identification of the role of the various scattering processes, respectively. To this end, the optoelectronic properties of the films have been studied as a function of film crystallinity, both optically by spectroscopic ellipsometry focusing on the Drude response and electrically by temperature-dependent Hall measurements. The main results of this study include the finding that in crystallized films only ionized impurity scattering from singly charged donors and optical phonon scattering are of importance and that the experimentally determined contribution of phonon scattering is indeed found to be about half of the value predicted by Preissler et al.[10] Furthermore, the analysis rules out the prevalence of doubly charged oxygen vacancies (V_O^{2+}) as dopant in crystallized In_2O_3:H, and the source of doping is attributed to interstitial (H_i^+) or substitutional (H_O^+) hydrogen. Even though only ~4% of the H atoms in a crystallized In_2O_3:H film are observed to be an active dopant, neutral defect scattering from inactive H dopants is found to be negligible or absent. The fact that inactive H does not contribute to scattering could explain why H, besides being a singly charged donor, allows for extremely high carrier mobilities.

EXPERIMENTAL SECTION

Sample Preparation. Si(100) wafers with a 430 nm thermal oxide were used as substrates. A seed layer of 20 cycles of ALD Al_2O_3 was deposited using trimethylaluminum (TMA) and H_2O in an Oxford Instruments OpAL ALD reactor at a substrate temperature of 100 °C. In_2O_3:H films of 75 nm thickness were subsequently deposited using InCp and a combination of both H_2O and O_2. All samples used in this study were codeposited in one run. Postdeposition annealing took place in a Jipelec rapid thermal anneal (RTA) in an inert N_2 atmosphere. Annealing temperatures were varied between 150 and 200 °C. Note that in order to ensure compatibility with SHJ solar cell processing, the maximum annealing temperature has been limited to 200 °C.[4]

Film Analysis. X-ray diffraction (XRD) measurements were used to evaluate the film crystallinity X_c at various stages of crystallization. This was done by comparison of the sum of the integrated peak areas I_{hkl} of the two main diffraction peaks (i.e., (222) and (400)) to the sum of the maximum peak areas $I_{hkl,max}$ of the fully crystallized sample.[12]

$$X_c = \frac{\sum_{hkl} I_{hkl}}{\sum_{hkl} I_{hkl,\max}} \quad (1)$$

Example XRD spectra at various stages of crystallization can be found in Supporting Information Figure S1.

Rutherford backscattering (RBS) and elastic recoil detection (ERD) were used to obtain absolute atomic densities of most notably indium, oxygen, and hydrogen. The oxygen and indium binding configurations were assessed from X-ray photoelectron spectroscopy (XPS).

The film optoelectronic properties were evaluated from Hall measurements in the Van der Pauw configuration and by spectroscopic ellipsometry (SE). The Hall mobility μ_{Hall} and carrier density $N_{e,Hall}$ were corrected using the Hall scattering factor R_H to obtain the effective mobility μ and N_e, according to $\mu = \mu_{Hall}/R_H$ and $N_e = N_{e,Hall} \times R_H$.[10] R_H was assumed to be constant at 1.03 for all the samples, as determined by Preissler et al. for the carrier densities of interest in this study.[10] SE was used to determine the thicknesses and optical constants of the films. For the SE analysis, the dielectric function in the measured photon energy range of 0.75–5.0 eV was modeled by a combination of a Tauc–Lorentz oscillator to account for absorption across the optical bandgap and a Drude oscillator to account for FCA in the infrared part of the spectrum.[16] From the Drude modeling, the unscreened plasma frequency E_p and optical mobility can be obtained. Note that in principle the optical mobility determined by SE and the electrical mobility obtained from Hall measurements need not be equal because these two techniques are sensitive to scattering phenomena at different length scales. Generally, the microscopic interaction distance of light with free carriers is smaller than the characteristic length scale for grain boundary scattering, and such scattering is thus not optically probed. In macroscopic Hall measurements, all scattering phenomena are probed. Therefore, comparison of the optical and electrical mobility yields information on the contribution of grain boundary scattering.[17]

DOI: 10.1021/acsami.5b04420
ACS Appl. Mater. Interfaces 2015, 7, 16723–16729

Additionally, by assuming that the optically probed electron density is equal to the carrier density obtained from Hall measurements (i.e., $N_{opt} = N_e$) the effective electron mass m^* can be calculated from the unscreened plasma frequency E_p and carrier density.[3]

$$m^* = \frac{\hbar^2 e^2 N_e}{m_e \varepsilon_o E_p^2} \quad (2)$$

In this equation, $\hbar$ is the reduced Planck's constant, e is the elementary charge, ε_0 is the vacuum permittivity, and m_e is the electron mass.

Besides being assessed by XRD, the crystallinity X_c has also been assessed by modeling the ellipsometry data using a Bruggeman effective medium approximation (EMA) model, constituted by the optical constants obtained from an as-deposited, an amorphous, and a fully crystallized In_2O_3:H layer. The optical constants of the amorphous and crystallized layer can be found in Supporting Information Figure S2. The percentage of crystallinity (i.e., crystalline fraction X_c) and the depolarization factor were used as fit parameters.

RESULTS AND DISCUSSION

Structural Changes upon Annealing of In_2O_3:H. To obtain information on the crystallization kinetics, the film crystallinity has been evaluated by both XRD, according to eq 1, and by SE modeling for a range of annealing temperatures. In Figure 1, the evolution of the crystalline fraction during annealing is displayed. It can be seen that there is an overall good agreement between the crystalline fractions determined by XRD and SE.

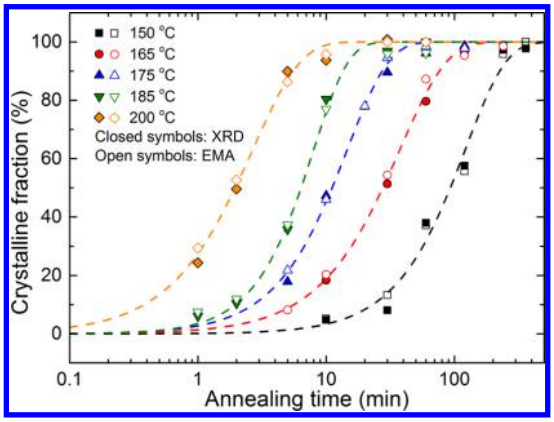

Figure 1. Crystalline fraction of In_2O_3:H films as a function of annealing time for various annealing temperatures. The crystallinity has been obtained from XRD (closed symbols) and SE modeling using an effective medium approximation (EMA, open symbols). The EMA consisted of the optical constants of fully crystalline and amorphous In_2O_3:H.

Crystallization is observed to occur more rapidly at higher annealing temperatures. At an annealing temperature of 200 °C, the film is fully crystallized after only 10 min, whereas it takes over 5 h to fully crystallize a film at 150 °C, indicating that crystallization is a thermally activated process. In Supporting Information Figure S3, cross-sectional TEM images of a fully crystallized sample are shown. In the next sections, the determined crystalline fractions X_c have been used to evaluate the evolution of the optoelectronic properties of the film as a function of crystallinity.

Changes in elemental composition during crystallization at 200 °C have been monitored by RBS and ERD, and the results have been summarized in Table 1. As can be seen, the films are slightly oxygen-rich with respect to bulk, single-crystal In_2O_3, and within experimental error, there is no change in the O/In ratio during annealing at 200 °C. A significant amount of hydrogen, 4.2 at. %, is incorporated in the film during deposition. Upon crystallization, a slight reduction in hydrogen content to 3.9 at. % is observed, presumably because of H_2 or H_2O effusion although the relative decrease (10%) is on the same order as the relative error in the determination of the hydrogen content (7%). The presence of OH bonds in amorphous and crystallized In_2O_3:H has also been confirmed by XPS from analysis of the O 1s signal (Supporting Information Figure S4).[18,19]

Table 1. Elemental Composition of In_2O_3:H Films Annealed at 200 °C as Obtained from RBS and ERD[a]

sample	[In] (at. %)	[O] (at. %)	[H] (at. %)	O/In ratio
as-deposited, amorphous	36.8	59.0	4.2	1.6
X_c = 24%	36.5	59.4	4.1	1.6
crystallized, X_c = 100%	37.1	59.0	3.9	1.6
stoichiometric In_2O_3	40	60	0	1.5

[a]The relative errors in the atomic percentages of In, O, and H are 2, 2, and 7%, respectively. The error in the O/In ratio is 3%.

Change in Optoelectronic Properties upon Crystallization. In addition to the change in structural properties, Hall and SE measurements have been performed on films of varying crystalline fraction X_c in order to gain insight into the evolution of the optoelectronic properties during crystallization. In Figure 2a the change upon crystallization in film carrier density N_e, as obtained from Hall measurements, and the plasma frequency E_p, as obtained from the ellipsometry modeling, are shown. As can be seen, the carrier density decreases from ~4.8 × 10 to ~1.8 × 10^{20} cm^{-3} during crystallization. A simultaneous reduction in plasma frequency E_p is observed from ~1.5 to ~1.0 eV because of a reduction of the carrier density.

The electrical mobility (Figure 2b) increases linearly with film crystallinity. This indicates that the measured Hall mobility is basically the average, weighted by X_c, of the electrical mobility values corresponding to the amorphous ($\mu_{e,a}$) and crystalline ($\mu_{e,c}$) phase. From the linear fit in Figure 2b, values of $\mu_{e,a}$ = 35 ± 1 $cm^2/(V\ s)$ and $\mu_{e,c}$ = 128 ± 4 $cm^2/(V\ s)$ have been determined. Because the increase in carrier mobility outweighs the decrease in carrier density, the film resistivity decreases from 0.35 mΩ cm for the as-deposited sample to as low as 0.26 mΩ cm for a fully crystallized sample. Interestingly, all the optoelectronic properties mainly depend on the film crystallinity irrespective of the annealing temperature used. This shows that at lower annealing temperatures In_2O_3:H can be obtained that is of quality as high as that obtained at higher annealing temperatures. This extends the applicability of the process to substrate materials that have more stringent requirements with respect to the thermal budget. Additionally, it should be noted that the samples showed excellent stability after 1 year of storage at room temperature.

The effective electron mass of amorphous (m_a^*) and crystallized (m_c^*) films has been determined using eq 2, in which the plasma frequency and carrier density were taken from Figure 2a. Values have been obtained that are in the range of values previously reported in literature: for the amorphous films, a value of m_a^* = 0.31 ± 0.01, and for the crystallized films, a value of m_c^* = 0.23 ± 0.02.[16,20−22] The reduction in effective mass upon crystallization is most likely due to a combination of

DOI: 10.1021/acsami.5b04420
ACS Appl. Mater. Interfaces 2015, 7, 16723−16729

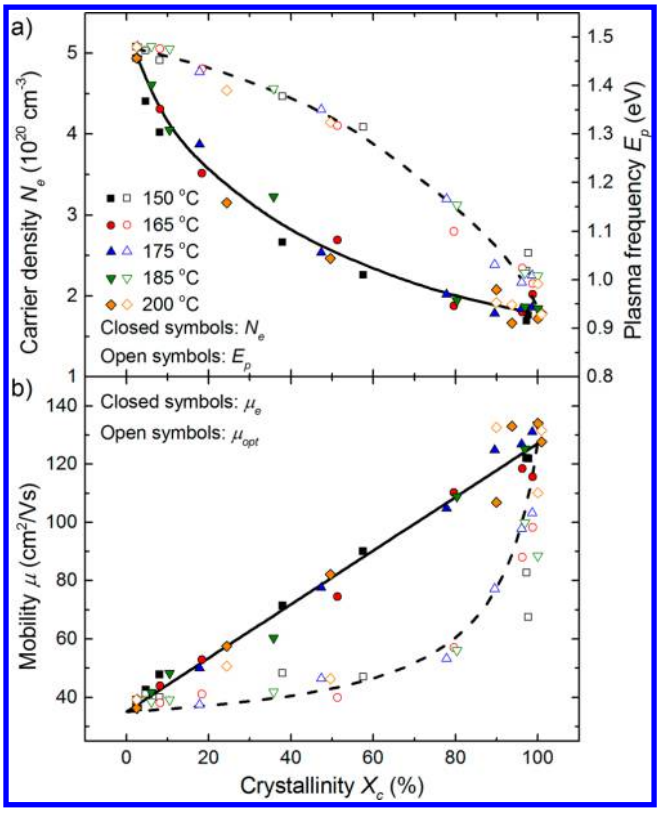

Figure 2. (a) Change in carrier density (closed symbol) as obtained from Hall measurements and plasma frequency (open symbol) as obtained from SE modeling for films of varying crystalline fractions annealed at various temperatures. The solid and dashed lines are guides to the eye. (b) Change in electrical mobility (closed symbol) and optical mobility (open symbol) during crystallization. The solid line is a linear fit of the electrical mobility, whereas the dashed line is generated using eq 3.

a reduction in carrier density and an alteration of the band structure.

The optical mobility, obtained from modeling the Drude oscillator in the ellipsometry data, shows very good agreement with the electrical mobility for the as-deposited and fully crystallized samples. Because scattering phenomena at length scales of grain boundary dimensions are not optically probed by ellipsometry, the fact that the optical and electrical mobility are equal implies that grain boundary scattering plays a negligible role in the crystallized films.[17] This statement can also be corroborated by comparison of the mean free path (MFP) of the charge carrier with the lateral grain size of a few hundred nanometer for crystallized In_2O_3:H films.[12] Using the Fermi velocity $v_F = \hbar(3\pi^2 N_e)^{1/3}/(m^* m_e)$ and the scatter frequency $\omega_\tau = e/(m^* m_e \mu_e)$, MFP = v_F/ω_τ has been found to be 15 nm for a fully crystallized sample.[17] Indeed, the length scale for grain boundary scattering greatly exceeds the MFP of the charge carrier. Additionally, the grain boundaries are most likely well-passivated by the available hydrogen.[19] Evidently, for the as-deposited samples, the optical and electrical mobility are equal because of the absence of grain boundary scattering in the amorphous material. However, for partly crystallized films the optical mobility is lower than the electrical mobility. This is in contrast to the common observation that depending on the presence of grain boundary scattering the optical mobility should either be equal or exceed the electrical mobility. This discrepancy can be explained by the fact that the film is modeled as a homogeneous medium in which only a single Drude oscillator is used to represent the scattering of electrons in both amorphous and crystalline In_2O_3:H phases. As seen from Figure 2a, the electron density belonging to the amorphous phase (~4.8×10^{20} cm^{-3}) is much higher than that belonging to the fully crystalline phase (~1.8×10^{20} cm^{-3}). Because all free electrons contribute equally to the Drude response, the higher electron density of the amorphous phase will weigh more strongly in the fitting of the effective scatter frequency (and hence to the optical mobility). Under the assumption that the fitted scatter frequency is weighted both by the volume fractions and carrier densities of the respective phases, the weighted optical mobility μ_{opt} for a given crystallinity X_c is represented as

$$\mu_{opt} = \mu_a \mu_c \frac{(1 - X_c)N_{e,a} + X_c N_{e,c}}{(1 - X_c)N_{e,a}\mu_c + X_c N_{e,c}\mu_a} \quad (3)$$

In this equation, the subscripts a and c denote the amorphous and crystalline phase, respectively. When inserting the carrier densities N_e and mobility μ of the amorphous and crystalline phase, as obtained by Hall measurements in eq 3, the dashed curve in Figure 2b is obtained. As can be seen, the trend in fitted optical mobility shows good agreement with eq 3. This confirms the aforementioned hypothesis, and it also demonstrates that for a proper evaluation of the mobility of a multicomponent material by optical means detailed knowledge of the material is prerequisite.

Mobility Limit and Doping Mechanism in In_2O_3:H. To distinguish between various scattering contributions in In_2O_3:H films, temperature-dependent Hall measurements have been performed on films of varying crystallinity X_c, as shown in the inset of Figure 3. As can be seen, the temperature dependence of the mobility of In_2O_3:H greatly varies with the film crystallinity. The carrier densities of the films did however

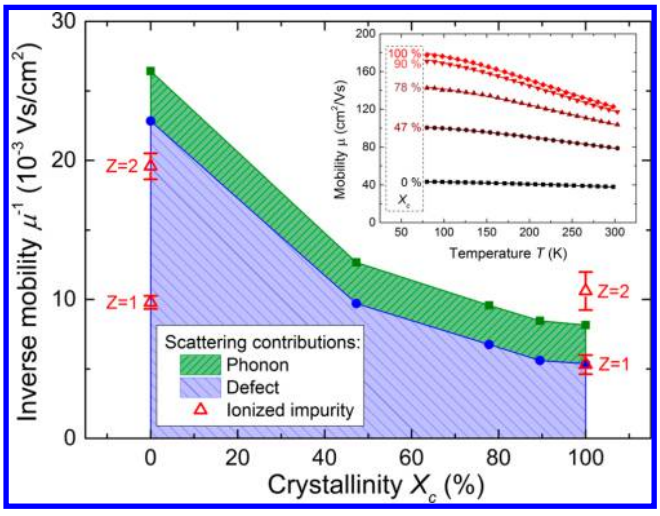

Figure 3. Inverse carrier mobility of In_2O_3:H films as a function of film crystallinity X_c. The contribution of phonon and defect scattering to the total scattering was obtained from the fits to the data in the inset. The ionized impurity scattering contributions of both singly ($Z = 1$) and doubly charged ($Z = 2$) donors in the amorphous and crystalline phases were calculated using eq 6. (Inset) Temperature-dependent carrier mobility of In_2O_3:H films of varying crystallinity, annealed at 175 °C. Solid lines are fits to the data using eq 5. The percentages denote the crystalline fraction X_c.

DOI: 10.1021/acsami.5b04420
ACS Appl. Mater. Interfaces 2015, 7, 16723−16729

not show a temperature dependence as expected given the degenerate nature of the semiconductor.

Because the various carrier scattering mechanisms have different temperature dependencies, their contributions to the total scattering can be extracted by fitting the temperature-dependent Hall data to an appropriate temperature-dependent mobility model. Defect scattering (including both ionized and neutral impurity scattering) is independent of temperature in a degenerate semiconductor, whereas phonon scattering follows a power law:

$$\mu_{\text{phonon}} = \mu_0 \left(\frac{T}{T_0}\right)^{-p} \tag{4}$$

In this equation, μ_0 denotes the phonon mobility at a reference temperature T_0. The parameter p is a parameter which should be either 1 if the temperature is above the Debye temperature or in the range of 2−4 if the temperature is below the Debye temperature.[23]

If the mobility is limited by a temperature-independent contribution from defect scattering (either neutral or ionized impurities) and a temperature-dependent contribution from phonon scattering, then the resulting temperature-dependent mobility can be expressed as follows, according to Matthiessen's rule:

$$\frac{1}{\mu(T)} = \frac{1}{\mu_i} + \frac{1}{\mu_0}\left(\frac{T}{T_0}\right)^{p} \tag{5}$$

In this equation, μ_i is the temperature-independent mobility caused by defect scattering. Note that grain boundary scattering is not explicitly taken into account in this expression. Given that the optical and electrical mobility for fully crystallized films are equal, it is expected that grain boundary scattering plays a negligible role. Additionally, at the carrier densities of interest, transport across grain boundaries will be mainly through tunneling instead of thermionic emission.[24] Because tunneling processes are temperature-independent, the grain boundary contribution would be contained in the temperature-independent mobility μ_i.

The temperature-dependent Hall data have been fitted using eq 5, which allows for the determination of the room-temperature phonon mobility μ_0 and defect scattering mobility μ_i. In all fits, the parameter p converged to values close to 2 and has therefore been fixed at 2. Reported values for the Debye temperature of In_2O_3 range from 420 to 811 K, and because all measurements were performed at lower temperatures, the value of p is within our expectation.[10,25,26]

In Figure 3, the contribution of phonon and defect scattering to the inverse mobility at various stages of crystallization has been plotted. By plotting the inverse mobility instead of the mobility, the different scattering contributions can be more readily visualized because they add linearly. As can be seen, the contribution of phonon scattering is rather constant during the crystallization process, whereas defect scattering decreases greatly upon crystallization. For reference, the calculated contribution of ionized impurity scattering to the inverse mobility because of either singly (Z = 1) or doubly (Z = 2) charged donors in amorphous and crystallized In_2O_3:H has been added. This has been calculated using eq 6:[27]

$$\mu_{ii} = \frac{3(\varepsilon_r\varepsilon_0)^2 h^3}{Z^2 m^{*2} e^3} \frac{N_e}{N_i} \frac{1}{F_{ii}^{np}(\xi_0)} \tag{6}$$

In this equation, h is Planck's constant, ε_0 and ε_r are the vacuum and relative permittivity, respectively, and $\xi_0 = (3\pi^2)^{1/3}\varepsilon_r\varepsilon_0 h^2 N_e^{1/3}/m^* e^2$. Z is the charge state of the ionized impurity, and N_i the concentration of ionized impurities (taken to be N_e/Z; i.e., full ionization is assumed). $F_{ii}^{np}(\xi_0)$ is the carrier-density-dependent screening function for ionized impurity scattering in a degenerate semiconductor.[28] The calculations were performed using the previously determined carrier densities and effective masses (and uncertainties therein) of the amorphous and crystalline phase and a relative permittivity of 8.9 for In_2O_3.[3]

A few key observations can be made from Figure 3. First, after crystallization the defect scattering contribution to the inverse mobility is much less than the limit for doubly charged donors (Z = 2), and within experimental error, ionized impurity scattering from singly charged donors (Z = 1) is the sole contributor to the total defect scattering. This proves that doubly charged donors, e.g., V_O^{2+}, cannot be the main electron donors for the crystallized films and that singly charged hydrogen in either an interstitial (H_i^+) or substitutional (H_O^+) site is the main electron donor after crystallization as was also predicted by density functional theory.[9] Interestingly, besides ionized impurity scattering from singly charged donors, the only other contribution to the inverse mobility for a fully crystallized film stems from phonon scattering (∼34%). This indicates that other defect scattering mechanisms (e.g., grain boundary scattering and neutral impurity scattering) play a negligible role in crystallized films and that the film mobility is limited by the fundamental phonon and ionized impurity scattering processes.

Second, the fitted phonon mobility value of the crystallized sample is around 360 $cm^2/(V\,s)$, which is higher than the value of ∼180 $cm^2/(V\,s)$ predicted by Preissler et al.[10] This is in line with their speculation that their model underestimates optical phonon scattering and explains the fact that experimental mobility values can exceed their predicted values.

Third, the mobility of the as-deposited amorphous samples is very close to the mobility limit because of ionized impurity scattering from doubly charged donors, calculated using the previously determined effective mass in amorphous In_2O_3:H. A similar observation was made by Koida et al., who suggested that this is due to the fact that ionized impurity scattering from doubly charged oxygen vacancies (V_O^{2+}) is the dominant scattering mechanism in amorphous In_2O_3:H made by sputtering.[3] The results in Figure 3 indicate that the same may apply to amorphous In_2O_3:H made by ALD, although from this data it cannot be concluded whether the mobility is solely limited by ionized impurity scattering from doubly charged donors. It is very well possible that also in amorphous films singly charged donors are prevalent and that other scattering mechanisms such as neutral impurity or defect scattering play an important role as well. Hence, the mobility increase during crystallization can be due to a reduction in other defect scattering mechanisms (e.g., neutral impurity) or due to a change from doubly charged donors to singly charged donors or a combination thereof.

Furthermore, using the concentration of hydrogen as obtained by ERD (4.9×10^{21} cm^{-3}), it has been calculated that only ∼3.7% of the incorporated H needs to serve as an active dopant in order to account for the carrier density of crystallized films (1.8×10^{20} cm^{-3}). Because neutral impurity scattering does not appear to play a major role, this suggests that inactive hydrogen (∼96.3%) in the In_2O_3:H matrix does

DOI: 10.1021/acsami.5b04420
ACS Appl. Mater. Interfaces 2015, 7, 16723−16729

not significantly contribute to scattering. In addition to the possibility of grain boundary passivation by hydrogen, this could very well be the main reason why H-doped films are capable of reaching much higher mobility values than typically obtained with Sn-doping.

CONCLUSIONS

In this work, the role of ionized impurity and optical phonon scattering, along with the doping mechanism in crystallized In_2O_3:H TCOs made by ALD has been established. It has been shown that irrespective of the annealing temperature films with excellent material properties are obtained after crystallization. From a comparison of the electrical and optical mobility of crystallized films, it has been found that grain boundary scattering does not play a significant role in these films. Additionally, the discrepancy between electrical and optical mobility for partly crystallized films has been explained by a difference in Drude response of the amorphous and crystalline parts of the mixed-phase material because of a difference in carrier density therein.

For fully crystallized films, the total scattering is dominated by optical phonon scattering and ionized impurity scattering from singly charged donors. Because these scattering processes are unavoidable, the mobility of the crystallized In_2O_3:H samples is at its upper limit for this specific carrier density. Additionally, the obtained optical phonon mobility exceeds the value predicted by Preissler et al., which confirms their suspicion of an underestimation of phonon scattering in In_2O_3.

Ionized impurity scattering of singly ionized dopants was found to be the only relevant defect scattering mechanism in crystallized films, which underlines the role of H as singly charged dopant in these films. The absence of any observable contribution of neutral defect scattering indicates that inactive H dopants do not contribute to a significant extent to defect scattering. This is a strong indication why H, besides being a singly charged donor, allows for extremely high carrier mobilities.

ASSOCIATED CONTENT

Supporting Information

X-ray diffraction spectra during crystallization at 175 °C, the optical constants of amorphous and crystallized In_2O_3:H, a high-resolution TEM image of crystallized In_2O_3:H, and X-ray photoelectron spectroscopy spectra of both amorphous and crystallized In_2O_3:H. The Supporting Information is available free of charge on the ACS Publications website at DOI: 10.1021/acsami.5b04420.

AUTHOR INFORMATION

Corresponding Author

*Tel.: +3140-247 4095. E-mail: b.macco@tue.nl.

Notes

The authors declare no competing financial interest.

ACKNOWLEDGMENTS

This work was financially supported by the Dutch Technology Foundation STW through the Flash Perspectief Programma. The research of W.M.M.K. has been made possible by the Dutch Technology Foundation STW and The Netherlands Organization for Scientific Research (NWO, VICI programma). We gratefully acknowledge C.A.A. van Helvoirt and C.O. van Bommel for technical assistance.

REFERENCES

(1) Ellmer, K.; Mientus, R. Carrier Transport in Polycrystalline Transparent Conductive Oxides: A Comparative Study of Zinc Oxide and Indium Oxide. *Thin Solid Films* **2008**, *516* (14), 4620−4627.
(2) Koida, T.; Fujiwara, H.; Kondo, M. Hydrogen-Doped In_2O_3 as High-Mobility Transparent Conductive Oxide. *Jpn. J. Appl. Phys.* **2007**, *46* (28), L685−L687.
(3) Koida, T.; Kondo, M.; Tsutsumi, K.; Sakaguchi, A.; Suzuki, M.; Fujiwara, H. Hydrogen-Doped In_2O_3 Transparent Conducting Oxide Films Prepared By Solid-Phase Crystallization Method. *J. Appl. Phys.* **2010**, *107* (3), 033514.
(4) De Wolf, S.; Descoeudres, A.; Holman, Z. C.; Ballif, C. High-Efficiency Silicon Heterojunction Solar Cells: A Review. *Green* **2012**, *2* (1), 7−24.
(5) Koida, T.; Fujiwara, H.; Kondo, M. Reduction of Optical Loss in Hydrogenated Amorphous Silicon/Crystalline Silicon Heterojunction Solar Cells by High-Mobility Hydrogen-Doped In_2O_3 Transparent Conductive Oxide. *Appl. Phys. Express* **2008**, *1*, 041501.
(6) Koida, T.; Fujiwara, H.; Kondo, M. High-Mobility Hydrogen-Doped In_2O_3 Transparent Conductive Oxide for a-Si:H/c-Si Heterojunction Solar Cells. *Sol. Energy Mater. Sol. Cells* **2009**, *93* (6−7), 851−854.
(7) Koida, T.; Sai, H.; Kondo, M. In_2O_3:H Transparent Conductive Oxide Films with High Mobility and Near Infrared Transparency for Optoelectronic Applications. *Surf. Eng.* **2012**, *28* (2), 102−107.
(8) Barraud, L.; Holman, Z. C.; Badel, N.; Reiss, P.; Descoeudres, A.; Battaglia, C.; De Wolf, S.; Ballif, C. Hydrogen-Doped Indium Oxide/Indium Tin Oxide Bilayers for High-Efficiency Silicon Heterojunction Solar Cells. *Sol. Energy Mater. Sol. Cells* **2013**, *115*, 151−156.
(9) Limpijumnong, S.; Reunchan, P.; Janotti, A.; Van de Walle, C. Hydrogen Doping in Indium Oxide: An Ab Initio Study. *Phys. Rev. B: Condens. Matter Mater. Phys.* **2009**, *80* (19), 193202.
(10) Preissler, N.; Bierwagen, O.; Ramu, A. T.; Speck, J. S. Electrical Transport, Electrothermal Transport, and Effective Electron Mass in Single-Crystalline In_2O_3 Films. *Phys. Rev. B: Condens. Matter Mater. Phys.* **2013**, *88* (8), 085305.
(11) Libera, J. A.; Hryn, J. N.; Elam, J. W. Indium Oxide Atomic Layer Deposition Facilitated by the Synergy between Oxygen and Water. *Chem. Mater.* **2011**, *23* (8), 2150−2158.
(12) Macco, B.; Wu, Y.; Vanhemel, D.; Kessels, W. M. M. High Mobility In_2O_3:H Transparent Conductive Oxides Prepared by Atomic Layer Deposition and Solid Phase Crystallization. *Phys. Status Solidi RRL* **2014**, *8* (12), 987−990.
(13) Macco, B.; Deligiannis, D.; Smit, S.; van Swaaij, R. A. C. M. M.; Zeman, M.; Kessels, W. M. M. Influence of Transparent Conductive Oxides on Passivation of a-Si:H/c-Si Heterojunctions as Studied by Atomic Layer Deposited Al-doped ZnO. *Semicond. Sci. Technol.* **2014**, *29* (12), 122001.
(14) Demaurex, B.; Seif, J. P.; Smit, S.; Macco, B.; Kessels, W. M. M. E.; Geissbuhler, J.; De Wolf, S.; Ballif, C. Atomic-Layer-Deposited Transparent Electrodes for Silicon Heterojunction Solar Cells. *IEEE J. Photovoltaics* **2014**, *4* (6), 1387−1396.
(15) Demaurex, B.; De Wolf, S.; Descoeudres, A.; Charles Holman, Z.; Ballif, C. Damage at Hydrogenated Amorphous/Crystalline Silicon Interfaces by Indium Tin Oxide Overlayer Sputtering. *Appl. Phys. Lett.* **2012**, *101* (17), 171604.
(16) Fujiwara, H.; Kondo, M. Effects of Carrier Concentration on the Dielectric Function of ZnO:Ga and In_2O_3:Sn Studied by Spectroscopic Ellipsometry: Analysis of Free-Carrier and Band-Edge Absorption. *Phys. Rev. B: Condens. Matter Mater. Phys.* **2005**, *71* (7), 075109.
(17) Knoops, H. C. M.; van de Loo, B. W. H.; Smit, S.; Ponomarev, M. V.; Weber, J. W.; Sharma, K.; Kessels, W. M. M.; Creatore, M. Optical Modeling of Plasma-Deposited ZnO Films: Electron Scattering at Different Length Scales. *J. Vac. Sci. Technol., A* **2015**, *33* (2), 021509.
(18) Purvis, K. K. L.; Lu, G.; Schwartz, J.; Bernasek, S. L. Surface Characterization and Modification of Indium Tin Oxide in Ultrahigh Vacuum. *J. Am. Chem. Soc.* **2000**, *122*, 1808−1809.

(19) Wardenga, H.; Frischbier, M.; Morales-Masis, M.; Klein, A. In Situ Hall Effect Monitoring of Vacuum Annealing of In_2O_3:H Thin Films. *Materials* **2015**, *8*, 561−574.
(20) Karazhanov, S.; Ravindran, P.; Vajeeston, P.; Ulyashin, a.; Finstad, T.; Fjellvåg, H. Phase Stability, Electronic Structure, and Optical Properties of Indium Oxide Polytypes. *Phys. Rev. B: Condens. Matter Mater. Phys.* **2007**, *76* (7), 075129.
(21) Hamberg, I.; Granqvist, C.; Berggren, K. Band-Gap Widening in Heavily Sn-Doped In_2O_3. *Phys. Rev. B: Condens. Matter Mater. Phys.* **1984**, *30* (6), 3240.
(22) Rosen, J.; Warschkow, O. Electronic Structure of Amorphous Indium Oxide Transparent Conductors. *Phys. Rev. B: Condens. Matter Mater. Phys.* **2009**, *80* (11), 115215.
(23) Das, A. K.; Misra, P.; Ajimsha, R. S.; Bose, a.; Joshi, S. C.; Phase, D. M.; Kukreja, L. M. Studies on Temperature Dependent Semiconductor to Metal Transitions in ZnO Thin Films Sparsely Doped with Al. *J. Appl. Phys.* **2012**, *112* (10), 103706.
(24) Zhang, D. H.; Ma, H. L. Scattering Mechanisms of Charge Carriers in Transparent Conducting Oxide Films. *Appl. Phys. A: Mater. Sci. Process.* **1996**, *62* (5), 487−492.
(25) Sobotta, H.; Neumann, H.; Kühn, G.; Riede, V. Infrared Lattice Vibrations of In_2O_3. *Cryst. Res. Technol.* **1990**, *25*, 61−64.
(26) Bachmann, K.; Hsu, F.; Remeika, J. The Low Temperature Heat Capacities of SnO_2 and In_2O_3. *Phys. status solidi* **1981**, *67*, K39−K42.
(27) Ellmer, K. Past Achievements and Future Challenges in the Development of Optically Transparent Electrodes. *Nat. Photonics* **2012**, *6* (12), 809.
(28) Pisarkiewicz, T.; Zakrzewska, K.; Leja, E. Scattering of Charge Carriers in Transparent and Conducting Thin Oxide Films with a Non-Parabolic Conduction Band. *Thin Solid Films* **1989**, *174*, 217−223.

DOI: 10.1021/acsami.5b04420
ACS Appl. Mater. Interfaces 2015, 7, 16723−16729